Construction of reporter and expression vectors

The 5′ flanking region of mouse *Tfr1* (from bp +16 to +436; +1 indicates the transcription start site) gene was amplified using Elongase Enzyme mix (Invitrogen) using DNA extracted from Colon 26 cells. PCR was performed using the forward primer 5′-AGTTGAGCTC(*SacI*)GGCTTGGTGCAGCTCAGTTAGTAG-3′ and reverse primer 5′-ATGAGATATC(*Eco*RV)TAAATGTCCGTTGACACTAGTAACC-3′. The PCR products were purified and ligated into a pGL4 Basic vector (*Tfr*1-Luc). The sequence of the CACGTG E-box (bp +290 to +295) on *Tfr1*-Luc was mutated using a QuikChange site-directed mutagenesis kit (Stratagene). Expression vectors for mouse CLOCK, BMAL1, and c-Myc were constructed using cDNAs obtained from RT-PCR derived from mouse liver RNA. All coding regions were ligated into the pcDNA3.1 (+) vector (Invitrogen), as previously described (7). Protein expression levels from each expression vector in Colon 26 were assessed by Western blotting analysis (Supplementary Data S2).

Luciferase reporter assay

Colon 26 cells were seeded at 3×10^5 cells per well in six-well culture plates (BD Biosciences). After an 18-hour culture, the cells were transfected with 100 ng per well of reporter vector and 2 μg per well (total) of expression vector using Lipofectamine LTX reagent (Invitrogen). A 0.5-ng-per-well sample of phRL-TK vector (Promega) was also cotransfected as an internal control reporter. The total amount of DNA per well was adjusted by adding pcDNA3.1 vector (Invitrogen). At 24 hours posttransfection, cells were harvested and the cell lysate was analyzed using a dual-luciferase reporter assay system (Promega). The ratio of firefly luciferase activity to *Renilla* luciferase activity in each sample served as a measure of normalized luciferase activity.

Small interfering RNA

siRNA of the mouse *c-Myc* gene was designed using BLOCK-iT RNAi Designer (Invitrogen). The siRNA oligonucleotide sequences were as follows: siRNA control sense, 5′-UAGUGUGAGCACUGUGAUUCCUUGG-3′ and antisense 5′-CCAAGGAUCACAGUGCUCACACUA-3′; *c-Myc* siRNA sense 5′-UAGUCGAGGUC-AUAGUUCCUGUUGG-3′ and antisense 5′-CCAACAGGAACUAUGACCUCGACUA-3′. The oligonucleotides were transfected into Colon 26 cells at a final concentration of 20 nmol/L using Lipofectamine 2000 (Invitrogen).

Chromatin immunoprecipitation assays

Tumor masses were excised and treated with 1% formaldehyde for 5 minutes at room temperature to cross-link the chromatin, and the reaction was stopped by adding glycine to a final concentration of 0.125 mol/L. Each cross-linked sample was sonicated on ice and then incubated with antibodies against c-MYC, CLOCK, rabbit-IgG, or goat-IgG (Santa Cruz Biotechnology). Chromatin/antibody complexes were extracted using a protein G agarose kit (Roche). DNA was isolated using the Wizard SV Genomic DNA Purification System (Promega) and subjected to PCR using the following primers for the c-MYC binding site (E-box) of the *Tfr1* promoter region, forward 5′-GTGACTCCCTTGTCAG-3′ and reverse 5′-CCGTGACACTAGTAACC-3′. For PCR analysis, PCR products were amplified for 40 or 45 cycles. PCR products were run on an agarose (3%) gel, including 0.2 μg/mL ethidium bromide, and analyzed using the NIH image software.

Determination of L-OHP (Pt) concentration

Plasma samples were obtained by centrifugation at 3,000 rpm for 3 minutes and stored at −20°C until analysis. Tumor DNA was extracted using a Wizard Genomic DNA Purification kit (Promega). Measurements of the L-OHP (Pt) content in plasma and tumor DNA were made using ICP-MS at the Center of Advanced Instrumental Analysis, Kyushu University. ICP-MS is capable of detecting very small amounts of Pt. Plasma Pt concentration and its tumor DNA content were expressed as micrograms per milliliter and nanograms per nanogram of DNA, respectively.

Determination of the antitumor effect

Seven days after the inoculation of Colon 26 cells into mice, a single injection of Tf-NGPE L-OHP (L-OHP: 0, 7.5 mg/kg, i.v.) or vehicle (9% sucrose) was given to tumor-bearing mice at 9:00 a.m. or 9:00 p.m. This dosage of Tf-NGPE L-OHP was selected based on a preliminary study (Supplementary Data S3). In all mice, the tumor volumes were measured every 3 days throughout the duration of the experiment.

Statistical analysis

ANOVA was used for multiple comparisons, and Scheffe's test was used for comparison between two groups. A 5% level of probability was considered significant.

Results

Twenty-four-hour rhythm in the expression of TfR1 in Colon 26 tumor masses

Two subtypes of TfR have been identified: TfR1 and TfR2. In implanted Colon 26 cells, *Tfr1* but not *Tfr2* was detectable, although *Tfr2* was expressed in mouse liver (Supplementary Data S1B). The protein and mRNA levels of TfR1 in implanted Colon 26 cells showed a significant 24-hour rhythm, with higher levels during the early dark phase ($P < 0.05$; Fig. 1A and B). The increase and decrease in mRNA levels of *Tfr1* seemed to cause the rhythm of TfR1 protein in Colon 26 tumor masses.

Regulation of the 24-hour rhythm in the expression of *Tfr1* gene by c-MYC

Among these, c-MYC is a potent activator of *Tfr1* gene transcription in mice and humans, and the transactivation effect was elicited through binding to the CACGTG E-box located in the first intron region (18, 19). In addition, CLOCK/BMAL1 heterodimers also bind cooperatively to CACGTG E-box sequences and regulate the rhythmic expression of their target genes (2). Thus, to establish the relevance of the biological clock system on the expression of *Tfr1*, CLOCKΔ19 (CLOCK protein lacking transcriptional activity) was overexpressed in Colon 26 cells. Clock mutant mice have

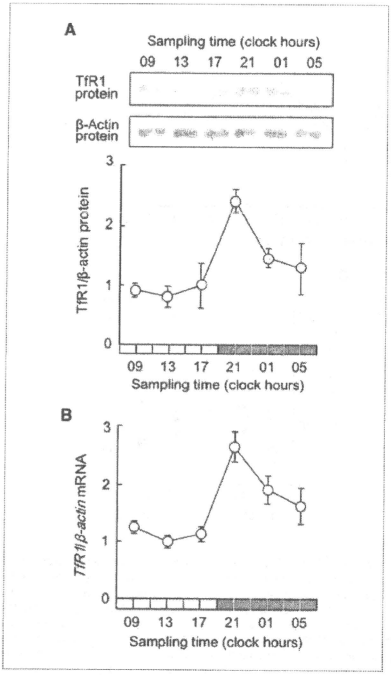

Figure 1. Twenty-four hour variation in the expression of TfR1 in Colon 26 tumor masses. A, temporal expression profile of TfR1 protein in tumor masses. The photographs show 24-h variation in TfR1 protein in implanted Colon 26 tumor cells. Cytoplasmic proteins were measured using each of the antibodies. Bottom, relative TfR1 protein levels. The data were normalized using β-actin as a control. Points, mean (n = 3, P < 0.01, ANOVA); bars, SEM. B, temporal expression profile of *TfR1* mRNA in tumor masses. The data are normalized using β-*actin* as a control. Points, mean (n = 6, P < 0.01, ANOVA); bars, SEM.

a point mutation in exon 19 of the *Clock* gene and exhibit low-amplitude rhythms in the expression of various genes (20). *TfR1* and *c-Myc* expression levels were low in CLOCKΔ19 overexpressing Colon 26 cells (Supplementary Data S4). Next, we tested whether these transcription factors participate in regulation of the rhythmic expression of *TfR1* gene in Colon 26 cells. Cotransfection of *TfR1*-Luc with c-MYC expression constructs resulted in an 8.1-fold increase in promoter activity, whereas CLOCK/BMAL1 had little effect on the transcriptional activity of the *TfR1* gene (Fig. 2B). The transactivation effect of c-MYC on *TfR1* reporters was dependent on the E-box element located from bp +290 to +295 because mutation of the CACGTG sequence to AAGCTT reduced transcriptional activation by c-MYC from 8.1- to 1.5-fold.

Several compounds and high concentration serum have been shown to induce and/or synchronize circadian gene expression in cultured cells (21). Thus, to elucidate the role of c-MYC in the circadian regulation of *TfR1* expression, the temporal expression profiles of *TfR1* mRNA in c-MYC–downregulated Colon 26 cells were investigated after 50% FBS treatment. Brief exposure of control scrambled siRNA-transfected cells to 50% FBS resulted in the oscillation of *TfR1* mRNA levels with a period length of ~24 hours (Fig. 3A). On the other hand, the protein levels of c-MYC were decreased and the mRNA levels of *TfR1* failed to show a significant 24-hour oscillation after the treatment of *c-Myc* siRNA–transfected cells with 50% FBS (Fig. 3B and C). These results suggested that c-MYC is required for generating the time-dependent variation in *TfR1* mRNA expression.

The transcription of *c-Myc* is regulated by components of the circadian clock, and its mRNA levels in mouse liver and bones have been shown to exhibit a significant 24-hour oscillation (22). The protein levels of c-MYC in Colon 26 cells implanted in mice also showed obvious 24-hour oscillations with higher levels around the early dark phase and lower levels during the early light phase, whereas there was no obvious 24-hour variation in the protein levels of CLOCK in the tumor

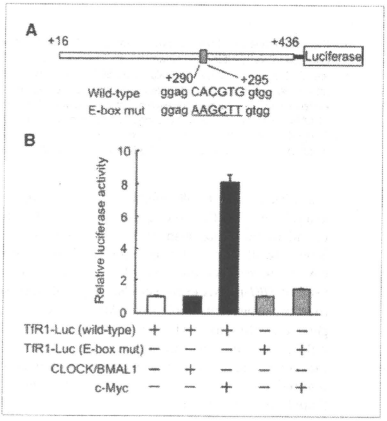

Figure 2. Influence of CLOCK/BMAL1 and c-MYC on transcription of the mouse *TfR1* gene. A, schematic representation of the mouse *TfR1* promoter. The numbers on both sites, the distance (bp) from the transcription start site (+1) included in the luciferase reporter construction. The numbers of nucleotide residues below the box, the positions of the E-box. The underlined nucleotide residues, the mutated sequence of the E-box. B, wild-type or E-box–mutated *TfR1* gene reporter plasmids (*TfR1*-Luc) were cotransfected with expression constructs encoding CLOCK/BMAL1 or c-MYC. Columns, mean (n = 3); bars, SEM.

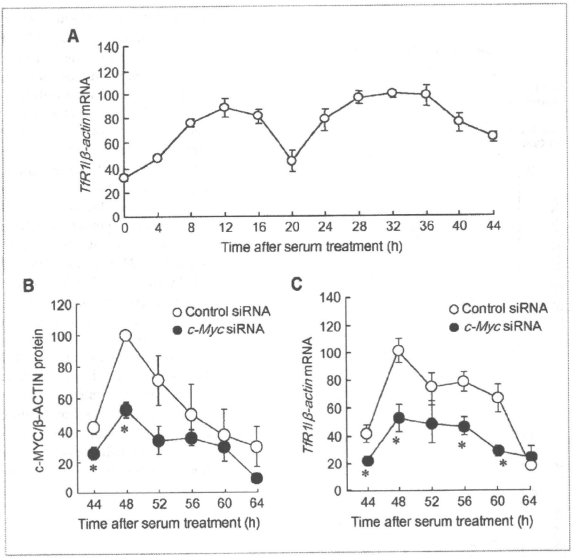

Figure 3. Influence of the downregulation of c-MYC on the rhythmic expression of *TfR1* mRNA in Colon 26 cells. A, temporal accumulation of *TfR1* mRNA in Colon 26 cells after 50% serum shock. The data are normalized using β-*actin* as a control. Points, mean ($n = 3$, $P < 0.01$, ANOVA); bars, SEM. Data are plotted relative to the 0-h value after 50% serum shock. B, temporal accumulation of c-MYC protein in control cells or c-Myc knockdown cells after 50% serum shock. Colon 26 cells were transfected with scrambled siRNA (control siRNA) or specific siRNA for c-Myc (c-Myc siRNA). Crude cell extracts were measured by Western blotting analysis. The data were normalized using β-actin as a control. Points, mean ($n = 3$, control cells; $P < 0.01$, ANOVA); bars, SEM. *; $P < 0.05$, when compared with the value for the control siRNA group at the corresponding times. C, temporal accumulation of *TfR1* mRNA in control cells or *c-Myc* knockdown cells. The mRNA levels of *TfR1* were determined at the indicated time points after serum treatment. Points, mean ($n = 3$, control cells; $P < 0.01$, ANOVA); bars, SEM. *, $P < 0.05$, when compared with the value for the control siRNA group at the corresponding times.

cells (Fig. 4A). The results of chromatin immunoprecipitation analysis revealed that endogenous c-MYC in Colon 26 cells bound to the E-box element in the intron region of *TfR1* gene (Fig. 4B). Of particular note, the binding amounts of c-MYC increasedat the time of day corresponding to the peak of *TfR1* mRNA expression (see Fig. 1B), suggesting that the time-dependent binding of c-MYC to the E-box in *TfR1* gene underlies its rhythmic expression. In addition, the mRNA levels of a prototypical c-MYC–regulated gene, telomerase reverse transcriptase (23), in Colon 26 cells implanted in mice also showed time-dependent variation (Supplementary Data S5).

Relationship between the rhythmic expression of TfR1 and time dependency of Pt incorporation into tumor DNA

Tf-NGPE L-OHP is a transferrin-conjugated liposome encapsulating L-OHP, a diaminocyclohexane Pt antitumor agent, which forms adducts with DNA. Tf-NGPE L-OHP binds to TfR, which is expressed on the plasma membrane and can internalize Pt into the cell.[3] Thus, to explore the function of internalization into the cell through transferrin in the rhythmic expression of TfR1, we investigated the temporal profile of *TfR1* gene expression and incorporation of Pt into tumor DNA in synchronized and desynchronized Colon 26 cells. A brief exposure of cultured Colon 26 cells to 50% FBS medium for 2 hours induced an oscillation in the expression of *TfR1* mRNA (Fig. 5A). The mRNA levels of *TfR1* peaked at 18 hours after treatment of the cells with 50% FBS. The oscillation of *TfR1* mRNA levels was also found on day 3 after serum treatment (see Fig. 3). The amount of Pt incorporated into the DNA of serum-shocked cells after treatment with Tf-NGPE L-OHP increased significantly at the time point corresponding to the peak in the level of TfR1 protein ($P < 0.05$; Fig. 5B). In contrast, in nontreated cells, neither the mRNA and protein levels of TfR1 nor Pt incorporation showed significant time-dependent variations (Fig. 5A and B), suggesting that the oscillation in the

[3] Our unpublished data.

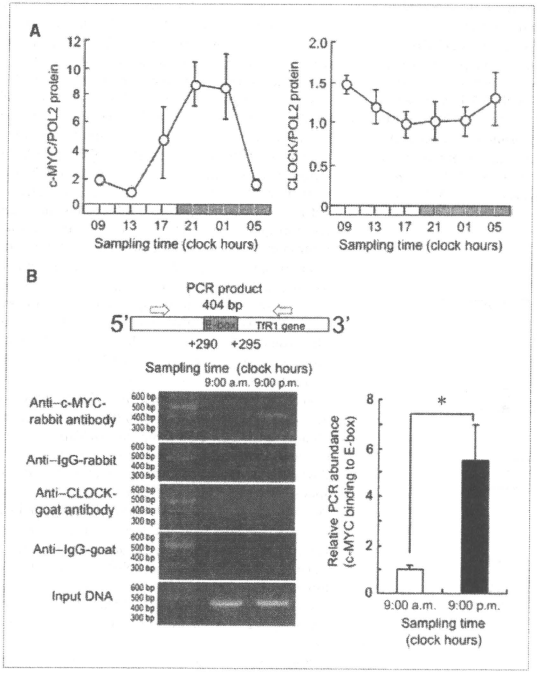

Figure 4. Time-dependent changes in the binding of endogenous c-MYC to the E-box element in the *TfR1* gene. A, temporal expression profiles of protein levels of c-MYC and CLOCK in implanted Colon 26 tumor masses. POL2 protein was used as an internal control whose expression was constant throughout the day. The data are normalized using POL2 as a control ($P < 0.01$, ANOVA). CLOCK protein did not show an obvious variation. Points, mean ($n = 3$); bars, SEM. B, left, temporal profiles of the binding of endogenous c-MYC to the *TfR1* gene in Colon 26 cells implanted in mice. Right, the quantification of temporal changes in the binding of c-MYC to the *TfR1* gene in Colon 26 cells implanted in mice. The mean value of each assay at 9:00 a.m. was set at 1. Columns, mean ($n = 3$); bars, SEM. *; $P < 0.05$ for the comparison between the two groups.

expression of TfR1 underlies the time-dependent change in Pt incorporation into tumor DNA.

Influence of dosing time on the ability of Tf-NGPE L-OHP to inhibit tumor growth

The plasma Pt concentration decreased gradually after a single injection of 7.5 mg/kg Tf-NGPE L-OHP (i.v.) at both dosing times, but the Pt concentration in plasma at 3 hours after Tf-NGPE L-OHP injection was significantly higher in mice injected with the drug at 9:00 a.m. than at 9:00 p.m. (Fig. 6A, left). On the other hand, Pt incorporation into DNA in tumor cells at 3 and 6 hours after Tf-NGPE L-OHP injection was significantly higher in mice injected with the drug at 9:00 p.m. than at 9:00 a.m. (Fig. 6A, right). We also attempted to determine the Pt contents in tumor DNA at over 6 hours after Tf-NGPE L-OHP injection, but accurate assessment was difficult, probably due to L-OHP–induced apoptotic or necrotic tumor cell death.

A significant antitumor effect of Tf-NGPE L-OHP was observed when tumor-bearing mice were injected i.v. with a single dose of 7.5 mg/kg L-OHP (Supplementary Data S3). Thus, the dosage was set at 7.5 mg/kg to investigate whether the antitumor effect of Tf-NGPE L-OHP was altered depending on its dosing time. The growth of tumor cells was significantly suppressed by the administration of Tf-NGPE L-OHP (7.5 mg/kg, i.v.). The antitumor effects were more potent in mice injected with the drug at 9:00 p.m. than in those that received it at 9:00 a.m. (Fig. 6B). Fifteen days after injection of the drug, the tumor volume in mice injected with Tf-NGPE L-OHP at 9:00 p.m. was significantly smaller than that in mice injected at 9:00 a.m. ($P < 0.05$).

Discussion

TfR1 is a key cell surface molecule that regulates the uptake of iron-bound transferrin (8). It has been shown that correlation exists between the number of surface TfR1 and the rate of cell proliferation. TfR1 expression is higher in tumor cells than in normal cells. Thus, intracellular targeting using iron-saturated Tf as a ligand for TfR-mediated endocytosis has attracted attention. In this study, the protein abundance of TfR1 on Colon 26 tumor cells implanted in mice showed a clear 24-hour oscillation. The rhythmic phase of TfR1 protein

paralleled that of its mRNA levels. However, the mechanisms of transcriptional rhythm of TfR1 were unclear.

The molecular circadian clock operates at a cellular level and coordinates a wide variety of physiologic processes (24). CLOCK/BMAL1 heterodimers activate the transcription of *Per, Cry,* and *Dec* genes through CACGTG E-box enhancer elements (8). The results of luciferase reporter assays and chromatin immunoprecipitation experiments revealed that the CACGTG E-box located in the first intron of the mouse *TfR1* gene was unable to respond to CLOCK/BMAL1 heterodimers. In contrast, as reported previously (19), c-MYC could bind to the E-box of the mouse *TfR1* gene and activate its transcription. The amount of endogenous c-MYC protein binding to the mouse *TfR1* gene E-box fluctuated in a time-dependent manner. The binding of c-MYC to the E-box increased at the time corresponding to the peak of *TfR1* mRNA expression, suggesting that c-MYC acts as a regulator of circadian expression of the *TfR1* gene in Colon 26 tumor cells. This hypothesis was also supported by the present findings that the amplitude of the *TfR1* mRNA rhythm in serum-shocked Colon 26 cells was decreased by the down-regulation of c-MYC. On the other hand, CLOCK protein did not bind to the *TfR1* gene E-box. This may account for the unresponsiveness of the *TfR1* gene to CLOCK/BMAL1 heterodimers. The sequence surrounding the E-box and its location had a marked influence on the transcriptional activity of CLOCK/BMAL1 (6). In fact, a CT-rich *cis*-acting element of the mouse vasopressin gene confers robust CLOCK/BMAL1 responsiveness on an adjacent E-box (25). The absence of such a CT-rich *cis*-acting element around the E-box may result in the inability of CLOCK/BMAL1 to transactivate the mouse *TfR1* gene.

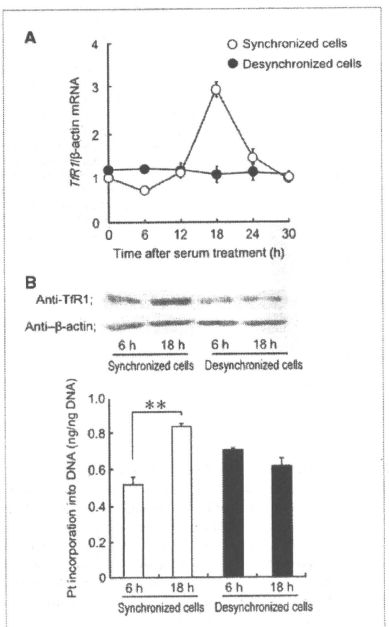

Figure 5. Influence of rhythmic changes in the expression of TfR1 on intratumoral delivery of L-OHP by Tf-NGPE liposomes. A, the temporal expression profile of *TfR1* mRNA in synchronized (○) or unsynchronized (●) Colon 26 cells. Cultured Colon 26 cells were synchronized by exposure to 50% FBS for 2 h. Points, mean ($n = 3$, synchronized cells; $P < 0.05$, ANOVA); bars, SEM. B, the photographs show temporal expression of TfR1 protein in synchronized or unsynchronized Colon 26 cells. Bottom, that temporal profile of Pt incorporation into DNA in synchronized or unsynchronized Colon 26 cells. Cells were exposed to Tf-NGPE L-OHP (L-OHP: 0.4 mg/mL) for 3 h at 6 or 18 h after the serum treatment, and then the amounts of Pt incorporated into tumor DNA were measured. Columns, mean ($n = 3$); bars, SEM. *, $P < 0.05$ for the comparison between the two time points.

Because the rhythmic phase of c-MYC protein abundance in Colon 26 cells correlated with the time dependency of its binding to the *TfR1* gene E-box, the oscillation in c-MYC protein levels may cause the 24-hour rhythm in the expression of downstream genes by rhythmic binding to their DNA response elements. In fact, *mTERT* mRNA in implanted Colon 26 tumor also showed time-dependent variation. In addition, *c-Myc* is regulated by clock genes, as indicated by previous results (26). *TfR1* and *c-Myc* expression levels were low in CLOCKΔ19-overexpressing Colon 26 cells. Although the E-box of the *TfR1* gene did not respond to CLOCK/BMAL1, the molecular components of the circadian clock may indirectly regulate the expression of the *TfR1* gene in Colon 26 cells.

It was reported previously that L-OHP could accumulate in tumor masses following delivery using Tf-PEG liposomes (16). TfR-targeting liposomes also bind to TfR on tumor cell surfaces and are internalized into the cells by receptor-mediated endocytosis. In this study, to evaluate the function of the 24-hour oscillation in TfR1, Tf-NGPE liposomes were used as a targeting carrier for intratumoral delivery of L-OHP. This TfR-targeting liposomal DDS exhibited similar pharmacokinetic properties to Tf-PEG liposomes, and i.v. administration of L-OHP encapsulated within Tf-NGPE liposomes lead to the accumulation of a high concentration of L-OHP in tumors as much as Tf-PEG liposomes.[4] The amount of Pt in tumor DNA after Tf-NGPE L-OHP injection increased at the times of day when TfR1 was abundant on the tumor surface in this study. This notion was also supported by *in vitro* findings that the time dependency of Tf-NGPE liposome–delivered L-OHP into tumor cells disappeared in the absence of the oscillation in TfR1 expression. These findings suggest that the oscillation in the expression of TfR1 underlies the dosing time–dependent changes in the internalization into

[4] Our unpublished data.

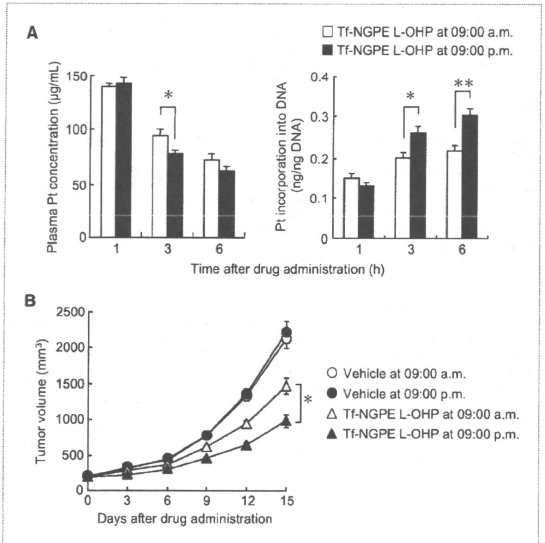

Figure 6. Influence of dosing time on the ability of Tf-PEG L-OHP to inhibit tumor growth in mice. Colon 26 tumor–bearing mice were injected i.v. with a single dose of Tf-NGPE L-OHP (L-OHP: 7.5 mg/kg) or vehicle (9% sucrose) at 9:00 a.m. or 9:00 p.m. A, dosing time–dependent differences in the intratumoral delivery of L-OHP by Tf-NGPE liposomes were examined. Plasma Pt concentration (left) and Pt incorporation into tumor DNA (right) were measured at the indicated times after an injection of Tf-NGPE L-OHP. Columns, mean (n = 5); bars, SEM; **, $P < 0.01$; *, $P < 0.05$ for comparison between the two groups. B, dosing time–dependent difference in the antitumor effect of Tf-NGPE L-OHP. Points, mean (n = 8–10); bars, SEM; *, $P < 0.05$ for comparison between the two dosing times.

the cells by receptor-mediated endocytosis. In addition, after a single injection of Tf-NGPE L-OHP, the antitumor effect of the drug varied according to its dosing time. The dosing time dependency of the antitumor effect seemed to be caused by time-dependent changes in the intratumoral delivery of L-OHP by TfR-targeting liposomes.

In the present study, it was shown that the 24-hour rhythm of TfR1 expression in colon cancer cells was controlled by c-MYC, and the cyclical accumulation of TfR1 caused dosing time–dependent changes in the intratumoral delivery of L-OHP by receptor-mediated endocytosis. Identification of the circadian properties of molecules that are targeted by ligand-directed DDS may aid the choice of the most appropriate time of day for their administration.

Disclosure of Potential Conflicts of Interest

The authors disclose no conflicts.

Grant Support

Grants-in-Aid for Scientific Research on Priority Areas "Cancer" (S.O. 20014016) from the Ministry of Education, Culture, Sport, Science and Technology of Japan, for Scientific Research (B; S.O. 21390047), for Challenging Exploratory Research (S.O. 21659041), and for the Encouragement of Young Scientists (N.M. 20790137) from the Japan Society for the Promotion of Science.

The costs of publication of this article were defrayed in part by the payment of page charges. This article must therefore be hereby marked *advertisement* in accordance with 18 U.S.C. Section 1734 solely to indicate this fact.

Received 01/18/2010; revised 06/07/2010; accepted 06/07/2010; published OnlineFirst 07/13/2010.

References

1. Stephan FK, Zucker I. Circadian rhythms in drinking behavior and locomotor activity of rats are eliminated by hypothalamic lesions. Proc Natl Acad Sci U S A 1972;69:1583–6.
2. Alvarez JD, Sehgal A. Circadian rhythms: finer clock control. Nature 2002;419:798–9.
3. Gekakis N, Staknis D, Nguyen HB, et al. Role of the CLOCK protein in the mammalian circadian mechanism. Science 1998;280:1564–9.
4. Kume K, Zylka MJ, Sriram S, et al. mCRY1 and mCRY2 are essential components of the negative limb of the circadian clock feedback loop. Cell 1999;98:193–205.
5. Preitner N, Damiola F, Lopez-Molina L, et al. The orphan nuclear receptor REV-ERBα controls circadian transcription within the positive limb of the mammalian circadian oscillator. Cell 2002;110:251–60.
6. Sato TK, Yamada RG, Ukai H, et al. Feedback repression is required for mammalian circadian clock function. Nat Genet 2006;38:312–9.

7. Koyanagi S, Kuramoto Y, Nakagawa H, et al. A molecular mechanism regulating circadian expression of vascular endothelial growth factor in tumor cells. Cancer Res 2003;63:7277–83.
8. Daniels TR, Delgado T, Helguera G, Penichet ML. The transferrin receptor part II: targeted delivery of therapeutic agents into cancer cells. Clin Immunol 2006;121:159–76.
9. Sorokin LM, Morgan EH, Yeoh GC. Transformation-induced changes in transferrin and iron metabolism in myogenic cells. Cancer Res 1989;49:1941–7.
10. Niitsu Y, Kohgo Y, Nishisato T, et al. Transferrin receptors in human cancerous tissues. Tohoku J Exp Med 1987;153:239–43.
11. Calzolari A, Oliviero I, Deaglio S, et al. Transferrin receptor 2 is frequently expressed in human cancer cell lines. Blood Cells Mol Dis 2007;39:82–91.
12. Kawabata H, Nakamaki T, Ikonomi P, Smith RD, Germain RS, Koeffler HP. Expression of transferrin receptor 2 in normal and neoplastic hematopoietic cells. Blood 2001;98:2714–9.
13. Röhrs S, Kutzner N, Vlad A, Grunwald T, Ziegler S, Müller O. Chronological expression of Wnt target genes Ccnd1, Myc, Cdkn1a, TfRc, Plf1 and Ramp3. Cell Biol Int 2009;33:501–8.
14. Papahadjopoulos D, Allen TM, Gabizon A, et al. Sterically stabilized liposomes: improvements in pharmacokinetics and antitumor therapeutic efficacy. Proc Natl Acad Sci U S A 1991;88:11460–4.
15. Ishida O, Maruyama K, Tanahashi H, et al. Liposomes bearing polyethyleneglycol-coupled transferrin with intracellular targeting property to the solid tumors *in vivo*. Pharm Res 2001;18:1042–8.
16. Suzuki R, Takizawa T, Kuwata Y, et al. Effective anti-tumor activity of oxaliplatin encapsulated in transferrin-PEG-liposome. Int J Pharm 2008;346:143–50.
17. Ohdo S, Koyanagi S, Suyama H, Higuchi S, Aramaki H. Changing the dosing schedule minimizes the disruptive effects of interferon on clock function. Nat Med 2001;3:356–60.
18. Holloway K, Sade H, Romero IA, Male D. Action of transcription factors in the control of transferrin receptor expression in human brain endothelium. J Mol Biol 2007;365:1271–84.
19. O'Donnell KA, Yu D, Zeller KI, et al. Activation of transferrin receptor 1 by c-Myc enhances cellular proliferation and tumorigenesis. Mol. Cell Biol 2006;26:2373–86.
20. Oishi K, Miyazaki K, Kadota K, et al. Genome-wide expression analysis of mouse liver reveals CLOCK-regulated circadian output genes. J Biol Chem 2003;278:41519–27.
21. Takiguchi T, Tomita M, Matsunaga N, Nakagawa H, Koyanagi S, Ohdo S. Molecular basis for rhythmic expression of CYP3A4 in serum-shocked HepG2 cells. Pharmacogenet Genomics 2007;17:1047–56.
22. Wittekindt NE, Hörtnagel K, Geltinger C, Polack A. Activation of c-*myc* promoter P1 by immunoglobulin κ gene enhancers in Burkitt lymphoma: functional characterization of the intron enhancer motifs κB, E box 1 and E box 2, and of the 3′ enhancer motif PU. Nucleic Acids Res 2000;28:800–8.
23. Reymann S, Borlak J. Transcription profiling of lung adenocarcinomas of c-*myc*-transgenic mice: identification of the c-*myc* regulatory gene network. BMC Syst Biol 2008;2:46.
24. Weaver ReppertSM. Coordination of circadian timing in mammals. Nature 2002;418:935–41.
25. Muñoz E, Brewer M, Baler R. Modulation of BMAL/CLOCK/E-Box complex activity by a CT-rich *cis*-acting element. Mol Cell Endocrinol 2006;252:74–81.
26. Fu L, Pelicano H, Liu J, Huang P, Lee C. The circadian gene Period2 plays an important role in tumor suppression and DNA damage response *in vivo*. Cell 2002;111:41–50.

DOSIMETRIC EVALUATION FOR NEUTRON CAPTURE THERAPY TO HEPATOCELLULAR CARCINOMA USING INTRA-ARTERIAL ADMINISTRATION OF BORON-ENTRAPPED WATER-IN-OIL-IN-WATER EMULSION

Hironobu Yanagie[1,2], Hiroaki Kumada[3], Takemi Nakamura[4],Syushi Higashi[5,6], Ichiro Ikushima[7], Yasuyuki Morishita[8],Atsuko Shinohara[9], Fijiwara Mitsuteru[10], Minoru Suzuki[11], Hirotaka Sugiyama[2], Tetsuya Kajiyama[6], Ryohei Nishimura[12], Koji Ono[11], Masazumi Eriguchi[2,13], and Hiroyuki Takahashi[1,2]

[1]Department of Nuclear Engineering & Management, Graduate School of Engineering, The University of Tokyo,Tokyo 113-8656,, [2]Cooperative Unit of Medicine & Engineering, The University of Tokyo Hospital, Tokyo 113-8655, [3]Proton Medical Research Center University of Tsukuba, Ibaraki 305-8575, [4]Japan Atomic Energy Rsearch Institute, Ibaraki 319-1184, [5]Department of Surgery, Ebihara Memorial Hospital, Miyazaki 885-0062, [6]Kyushu Industrial Sources Foundation, Miyazaki 885-0062, [7]Department of Radiology, Miyakonojyo Metropolitan Hospital, Miyazaki 885-0062, [8]Department of Human & Molecular Pathology, Graduate School of Medicine, The University of Tokyo, Tokyo 113-8655, [9]Department of Humanities, The Graduate School of Seisen University, Tokyo 141-8642, [10]SPG Techno Ltd. Co., Miyazaki 880-0303, [11]Research Reactor Institute, Kyoto University, Osaka 590-0494, [12]Department of Veternary Surgery, The University of Tokyo Veternary Hospital, Tokyo 113-0033, [13]Department of Surgery, Shin-Yamanote Hospital, Saitama 189-0021, JAPAN

Corresponding Author: Hironobu Yanagie, MD, PhD
Department of Nuclear Engineering & Management,Graduate School of Engineering, The University of Tokyo

Address: 7-3-1 Hongo, Bunkyo-ku, Tokyo, 113-8656 JAPAN
TEL: +81-3-5800-9194, FAX: +81-3-5800-9195,
E-mail: yanagie@n.t.u-tokyo.ac.jp

ABSTRACT

Hepatocellular carcinoma (HCC) is one of the difficult to cure with combinational medical therapies. Tumour cell destruction in boron neutron capture therapy (BNCT) is due to the nuclear reaction between ^{10}B atoms and thermal neutrons, so it is necessary to accumulate efficient ^{10}B atoms to tumour cells for effective BNCT. We prepared ^{10}BSH entrapped Water-in-oil-in-water(WOW) emulsion for selective intra-arterial infusion to HCC, and performed preliminary dosimetry with Japan Atomic Research Institute Computational Dosimetry System using CTscan imaging of HCC patient.

The ^{10}B concentrations in VX-2 tumour by WOW emulsion was superior to those by conventional emulsion. According to the rabbit model, the boron concentrations (ppm) of tumour, normal liver tissue, or blood is 61.7, 4.3, 0.1, respectively. In the epithermal lneutron dosimetry, the maximum tumour RBE dose, minimum tumour RBE dose, and mean tumour RBE dose are 43.1, 7.3, and 21.8 Gy-Eq, respectively, with the normal liver RBE restriction to 4.9 Gy, in 40 minutes irradiation. In this study, we showed that ^{10}B entrapped WOW emulsion would be applied to novel intra-arterial boron delivery carrier on BNCT to cancer, and, we showed the possibility to apply BNCT to HCC.

KEY WORDS

Boron Neutron-Capture Therapy (BNCT), Water-in-Oil-in-Water (WOW) Emulsion, Hepatocellular Carcinoma (HCC), Japan Atomic Energy Research Institute Computational Dosimetry System (JCDS)

1. Introduction

The cytotoxic effect of boron neutron capture therapy (BNCT) is due to a nuclear reaction between ^{10}B atom and thermal neutrons ($^{10}B + {}^{1}n \rightarrow {}^{7}Li + {}^{4}He$ (α) + 2.31 MeV (93.7 %) / 2.79 MeV (6.3 %)). The resulting lithium ions andαparticles are high linear energy transfer (LET) particles which produce high biological effects. These particles (α and ^{7}Li) destroy cells within about 10μm path length from the site of the capture reaction. It is theoretically possible to kill tumour cells without affecting adjacent healthy cells, if the former can selectively accumulate ^{10}B atoms. So it is very important to develop selective boron delivery systems for effective BNCT therapy [1,2,3,4]. BNCT is performed in patients with malignant brain tumours, melanoma, head & neck cancer [5]. We would like to apply BNCT, to radioresistant conditions as locally advanced or local recurrence of breast cancer, hepatocellular carcinoma, metastatic liver tumour, or lung cancer [6,7].

Most of hepatocellular carcinomas (HCC) are thought to be incurable, and limited surgical operation, chemotherapy, or radiation therapies are available for a prolonged survival. Iodized poppy-seed oil (IPSO) has a property of depositing itself selectively in the cells of HCC.

Higashi et al prepared a long term inseparable, water-in-oil-water emulsion (WOW) for use in arterial injection therapy to treat patients with HCC [8]. The WOW was prepared by membrane emulsification technique using a controlled pore glass [9]. Emulsification using a fine-pore glass membrane of equal pore size (i.e., controlled-pore glass membrane) is a new technique for preparing lipid microdroplets of equal size (monodispersed) containing aqueous fine microdroplets to form WOW emulsion. They also prepared a long term inseparable, WOW emulsion (WOW) containing 8-60 mg of epirubicin for use in arterial injection therapy for patients with HCC [10]. They reported that tumour size of HCC was reduced in six of seven patients, and a 50% or greater decrease of initial alpha-fetoprotein (AFP) levels was observed within 14 days in all four patients showing abnormal levels of serum AFP before treatment [10].

According to their clinical results, here we introduced BNCT to treatment of HCC for increasing the choice of therapies of HCC's patients. In this study, we developed boron compound entrapped WOW emulsion and evaluated its efficiency of selective boron delivery to cancer tissues. We also evaluate neutron flux dosimetry in frontal irradiation position of BNCT simulation for a HCC patient with CTscan images using JCDS at Japan Atomic Energy Research Institute.

2. Materials and Methods

2.1 Preparation of Boron compound entrapped WOW emulsion

Five hundred milligrams of $^{10}B_{12}H_{11}SH$ (^{10}BSH) was dissolved in 5 ml of 5% glucose solution, filtrated though controlled pore glass membrane emulsifying into 5 ml of IPSO containing surfactant, and then formed the water-in-oil emulsion (WO). Therefore, the WO emulsion was emulsifying again with aqueous phase containing 5 ml of saline and surfactant. The ^{10}BSH-entrapped WOW emulsion was prepared with the double emulsifying technique, [11].

The distributions of particle size of the vesicles of WOW and IPSO microdroplets were determined with a laser-diffraction particle-size analyzer SALD-2000 (Shimadzu Corp., Kyoto, Japan). The concentration of boron entrapped in WOW vesicles was determined by ICP-Mas- spectroscopy of Juntendo University.

Rabbit VX-2 cells (Shope-virus derived Squamous Cell Carcinoma cell line) were inoculated into the left lobe of liver [12]. Two weeks after tumour inoculation, WOW emulsions were administrated with arterial injections via proper hepatic artery on VX-2 rabbit hepatic tumour models. The results were compared with those of ^{10}BSH-IPSO mix emulsion. The boron concentrations of the tumour nodules and normal liver tissues were measured on one, or three days after arterial injections.

2.1 Neutron dosimetry with Japan Atomic Energy Research Institute Computational Dosimetry System (JCDS) for a HCC cancer patient

Neutron dosimetry for BNCT was performed to a patient with a 7 cm tumour in the left lobe of liver. LiF collimation was used to selectively irradiate the tumor while sparing the adjacent normal organs. The Neutron Beam Facility at JRR4 enables to carry out boron neutron capture therapy with epithermal neutron beam. The JAERI Computational Dosimetry System (JCDS), which can estimate distributions of radiation doses in a patient's head by simulating in order to support the treatment planning for epithermal neutron beam BNCT, was developed [13]. We applied this JCDS for evaluation the neutron dosimetry for this case.

3. Results and Discussion

We prepared ^{10}BSH entrapped WOW emulsion. The mean ^{10}B concentration was 13000 ppm by ICP-MAS. The size of WOW emulsion was controlled to 70 μ m (Figure 1- A & B).

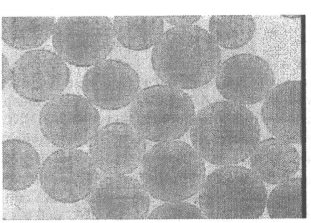

Figure 1-A. Microphotograph of WOW emulsion

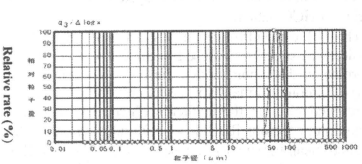

Figure 1-B. Particle size distribution of ^{10}BSH entrapped WOW emulsion by SALD-2000.

The ^{10}B concentration in VX-2 tumour was 141 ppm and 61 ppm at day 1 and day 3 respectively after arterial injection of WOW emulsion. The ^{10}B concentration of

tumour was 58 and 24ppm day1, day3, respectively after injection of IPSO mix emulsion (Table 1).

The histological staining delineated the superior accumulation of the fat doroplets of WOW emulsion in tumour site compared with lipiodol mix emulsion. Electro-microscopic figures of WOW emulsion proved the accumulation of fat droplets of WOW emulsion in the tumour site, but there was no accumulation of fat droplets in IPSO mix emulsion (data not shown). These results indicate that ^{10}B entrapped WOW emulsion selectively delivered and reserved the boron atoms to the cancer cell in tumour tissues, so the WOW emulsion is most useful for arterial boron delivery carrier on BNCT to cancer.

Table 1
^{0}B concentration of VX-2 hepatic tumour in rabbit model after arterial injection of ^{10}B-WOW emulsion or ^{10}B-IPSO mix emulsion

WOW	Tumour	Normal Liver	Blood
Day-1	141.8	6.1	1.2
Day-3	61.7	4.3	0.1

IPSO	Tumour	Normal Liver	Blood
Day-1	58.0	14.6	0.4
Day-3	24.5	3.9	0.2

The ^{10}B concentrations of samples were determined by ICP-masspectroscopy of Juntendo University.

Kumada et al had reported that JCDS is a software that creates a 3-dimensional head model of a patient by using CT scan and MRI images, and that generates a input data file automatically calculation of neutron flux and gamma-ray dose distributions in the brain with the Monte Carlo code MCNP, and that displays these dose distributions on the head model for dosimetry by using the MCNP calculation results [13]. JCDS has the following advantages; (1) a detailed 3D model of the patient's head can be easily obtained from the CT and MRI data, (2) the three-dimensional head image is editable to simulate the state of a head after surgery, (3) JCDS can provide information for the Patient Setting System which can support to set the patient to an actual irradiation position swiftly and accurately.

We performed the dosimetry with JCDS in the condition of BNCT using epithermal neutron beams(Figure 2). To decrease side effects to neighbor normal organs, the RBE dose to normal liver limited to 4.9 Gy-Eq, the RBE dose to left lung limited to 2.3 Gy-Eq, the RBE dose to right lung limited to 2.9 Gy-Eq, and the max skin RBE dose limited to 3.2 Gy-Eq, according to the experience of BNCT for HCC by Suzuki et al. The minimum tumour RBE dose is 7.3 Gy-Eq, the mean tumour RBE dose is 21.8 Gy-Eq, and the maximum tumour RBE dose is 43.1 Gy-Eq (Figure 3). For calibration of the beam peaks to tumour, it is necessary to perform the operative BNCT irradiation with addition of some void to the spread the neutron beams to tumours. We applied the JCDS to dosimetry of epithermal neutron, direction of neutron beam, and patient's positioning on BNCT. We also evaluate the epithermal neutron dose to decrease the side effects on neighbor normal tissues, for example, normal liver, lung, heart, skin, etc. High resolution whole body dosimetry system, as JCDS will be very useful to evaluate the thermal neutron dosimetry and the application of BNCT to multiple and/or advanced hepatic cancers.

Pinelli et al had reported that application of BNCT to liver tumours with developed a novel method for delivering sufficient and homogenous thermal fluence to the whole liver [14]. In their study, a patient suffering multiple liver metastases from colon cancer was treated with BNCT. The liver was surgically removed and transported to a reactor for irradiation with thermal neutrons, and then, the liver was auto- transplanted to the patient after BNCT irradiation. Suzuki et al have reported that intra- arterial delivery of a boron compound with a vessel embolizing agent (e.g. iodinated oil or IPSO) enables such highly selective accumulation of large amounts of boron compounds in rat liver tumours [15]. Suzuki et al had reported that the intra-arterial administration of a boron compound with IPSO is technically an application of chemoembolization, which has been widely used for the treatment of liver tumours [16].

4. Conclusion

According to clinical administration of WOW emulsion, drug encapsulating anti-cancer reagent in inner droplets, was significantly effective for both terminal and multi-originated in HCC when the drug was injected to suffered liver through a catheter inserted in liver artery. With ^{10}B entrapped in WOW emulsion it is possible to deliver and retain boron atoms in cancer cells in tumor tissues. These results show that ^{10}B entrapped WOW emulsions are most useful for arterial boron delivery for BNCT of cancer. We are now ongoing to plan clinical trials of BNCT for HCC patients, and hope to perform the first BNCT trial with WOW emulsions in the near future.

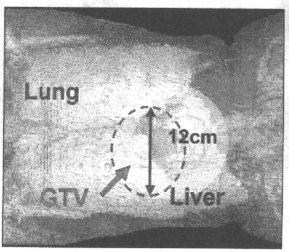

A

Figure 2.

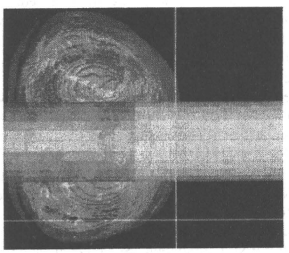

B

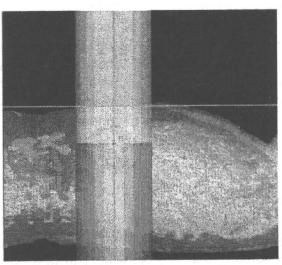

C

Figure 2. JCDS simulation for patient with HCC at the left lobe of liver. A : frontal view, B & C : lateral view

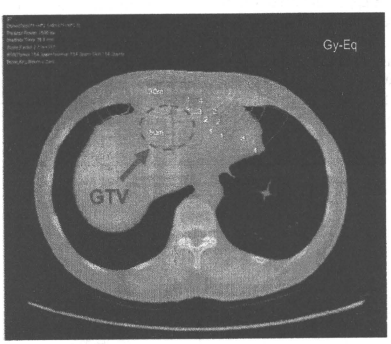

Figure 3. Distribution of tumour dose of epithermal neutron beam at JRR4 using JCDS evaluation for patient with HCC in left lobe of liver.

References

[1] Yanagie H, Tomita T, et al : Application of boronate anti-CEA immunoliposome to boron neutron capture therapy model, Brit. J. Cancer, 3(4): 522 - 526, 1991.

[2] Yanagie H, Tomita T, et al : Inhibition of human pancreatic cancer growth in nude mice by boron neutron capture therapy, British Journal of Cancer, 75 (5) : 660 - 665 ,1997.

[3] Yanagie H, Ogura K, et al : Accumulation of boron compound of tumor with polyethylene- glycol binding liposome by using neutron capture autoradiography, Applied Radiation and Isotopes, 61:639-646, 2004.

[4] Yanagie H, Maruyama K et al : Application of boron-entrapped stealth lipsomes to inhibition of growth of tumor cells in the in vivo boron neutron-capture therapy model, Biomed & Pharmacother, 60 : 43-50, 2006.

[5] Ono K., Masunaga S, Kinashi Y, and Takagaki M: Results of BNCT to Brain Tumors in KUR. Research and Development in Neutron Capture Therapy, Sauerwein et al.(Eds), Monduzzi Editore, Bologna, pp1097- 1100, 2002.

[6] Yanagie H, Kumada H, Sakurai Y, Nakamura T, Furuya Y, Sugiyama H, Ono K, Takamoto S, Eriguchi M, Takahashi H : Dosimetric evaluation of neutron capture therapy for local advanced breast cancer, Applied Radiation and Isotopes. 67 : S63–S66, 2009.

[7] Yanagie H, Sakurai Y, Ogura K, Kobayashi T, Furuya Y, Sugiyama H, Kobayashi H, Ono K, Nakagawa K, Takahashi H, Eriguchi M : Evaluation of neutron dosimetry on pancreatic cancer phantom model for application of intraoperative boron neutron-capture therapy. Biomedicine & Pharmacotherapy 61 (9), 505–514, 2007.

[8] Higashi S, Shimizu M, Setoguchi T : Preparation of new lipiodol- emulsion containing water soluble anticancer agent by membrane emulsification technique (In Japanese with English abstract), Drug Delivery System, 8 : 59-61, 1993.

[9] Nakashima T, Shimizu M, Kukizaki M : Membrane emulsification by micropolus glass, *Inorgan Membr.* ICIM2-92, 511-516, 1991.

[10] Higashi S, Shimizu M, Nakashima T, Iwata K, Uchiyama F, Tateno S, Tamura S, Setoguchi T : Arterial-Injection Chemo- therapy for Hepatocellular Carcinoma Using Monodispersed Poppy-Seed Oil Microdoloplets Containing Fine Aqueous Vesicles of Epirubicin, *Cancer*, 75 : 1245-1254, 1995.

[11] Nakashima T, Shimizu M & Kukizaki M : Development of Membrane Emulsification and Its Applications to Drug Delivery Systems(In Japanese with English abstract), *Maku (Membrane)*, 24, 278-289, 1999.

[12] Burgener FA : Peritoneal hepatic artery embolization in rabbits with VX2 carcinoma of the liver, *Cancer*, 46:56-63, 1984.

[13] Kumada H, The Development of a Computational Dosimetry System for BNCT at JRR-4. Frontiers in Neutron Capture Therapy, Hawthorne et al. (Eds), Kluwer Academic, New York, pp611-614, 2001.

[14] Pinelli T, Zonta A, Altieri S, Barni S, Braghieri A, Pedroni P, et al.: TAOrMINA: from the first idea to the application to the human liver. In: Sauerwein MW, Moss R, Wittig A editors. Research and Development in Neutron Capture Therapy. Bologna: Monduzzi Editore, International Proceedings Division, 1065–72, 2002.
[15] Suzuki M, Masunaga S, Kinashi Y, Nagata K, Sakurai Y, Nakamatsu K, et al : Intra-arterial administration of sodium borocaptate (BSH)/lipiodol emulsion delivers B-10 to liver tumors highly selectively for boron neutron capture therapy: experimental studies in the rat liver model. Int J Radiat Oncol Biol Phys, 59:260–6, 2004.
[16] Suzuki M, Sakurai Y, Hagiwara S, Masunaga S, Kinashi Y, Nagata K, Maruhashi A, Kudo M, and Ono K : First Attempt of Boron Neutron Capture Therapy (BNCT) for Hepatocellular Carcinoma. Jpn J Clin Oncol. 37(5):376- 81, 2007.

Expert Opinion

Hypoxia-inducible factor inhibitors: a survey of recent patented compounds (2004 – 2010)

Hyun Seung Ban, Yoshikazu Uto & Hiroyuki Nakamura†
†*Gakushuin University, Department of Chemistry, Faculty of Science, 1-5-1, Mejiro, Toshima-ku, Tokyo, 171-8588, Japan*

Introduction: Hypoxia-inducible factor (HIF) is a heterodimeric transcription factor consisting of α and β subunits that regulates the expression of angiogenic factors, including VEGF, which are involved in angiogenesis, invasion/metastasis, glucose uptake and cell survival during cancer development.
Areas covered: This review summarizes the information about patented HIF inhibitors over the last 7 years (2004 – 2010). The reader will gain an outline of the structure and biological activity of recently developed HIF inhibitors.
Expert opinion: Inhibition of HIF is an attractive therapeutic target for tumor angiogenesis and, until now, various HIF inhibitors have been discovered and evaluated. It is expected that development of more potent and selective HIF inhibitors will provide an effective treatment of cancer and other HIF-related diseases, including inflammation and cardiovascular disorder. As VEGF plays an important role in angiogenesis during tumor growth and ischemic diseases, the inhibition of VEGF-induced HIF is an attractive approach for the suppression of hypoxia-mediated pathological angiogenesis. HIF inhibitors may not only have cytostatic antitumor effects with fewer side effects, but also synergetic effects combined with radiotherapy.

Keywords: angiogenesis, cancer, HIF, HIF inhibitors, hypoxia

Expert Opin. Ther. Patents [Early Online]

1. Introduction

Hypoxia-inducible factor (HIF), a member of Per-aryl hydrocarbon receptor nuclear translocator (ARNT)-Sim family of heterodimeric basic helix-loop-helix transcription factor, consists of α subunits (HIF-1α, -2α and -3α) and β subunit (HIF-1β, which is also known as ARNT) [1-3]. Under aerobic condition, post-translational hydroxylation of proline residues (Pro402 and Pro564) in the oxygen-dependent degradation domain of HIF-1α is induced by oxygen-sensitive dioxygenases catalyzing prolyl hydroxylase (PHD). The hydroxylated HIF-1α binds to the von Hippel-Lindau (VHL) tumor suppressor protein, a component of the E3 ubiquitin ligase complex [4-7]. These interactions lead to the rapid degradation of HIF-1α through an ubiquitin and proteasome-dependent pathway [8-10]. Beside proline hydroxylation, asparagine (Asn803) in the C-terminal transactivation domain (CAD) of HIF-1α is hydroxylated by the factor-inhibiting HIF (FIH), an oxygen-dependent hydroxylase enzyme under aerobic condition [11]. This modification inhibits HIF transcriptional activity by preventing the interaction between CAD and p300/CBP transcriptional co-activator. Under hypoxic condition, HIF-1α is stabilized due to hypoxia-mediated reduction of PHD and FIH activities and is translocated into the nucleus, where it dimerizes with the constitutively expressed HIF-1β [12,13]. The HIF-1α and -β heterodimers bind to a *cis*-acting regulatory element referred to as

informa
healthcare

10.1517/13543776.2011.547477 © 2011 Informa UK, Ltd. ISSN 1354-3776

Article highlights.

- The hypoxia-inducible factor (HIF) is a heterodimeric transcription factor consisting of α and β subunits that take part in the expression of hypoxia-responsive genes involved in angiogenesis, invasion/metastasis, glucose uptake and cell survival during cancer development.
- As VEGF plays an important role in angiogenesis during tumor growth and ischemic diseases, the inhibition of VEGF-induced HIF is an attractive approach for the suppression of hypoxia-mediated pathological angiogenesis.
- HIF-1 inhibitors interfere with HIF-1α synthesis, folding, stabilization and nuclear transduction.
- The most important HIF-1α regulatory systems are PI3K/Akt/mTOR, MAPK, the HSP90 system, topoisomerase I and Trx-1, and clinical trials have been carried out with several HIF-1 inhibitors, including tenaspimycin, PX-866, PX-12, EZN-2968 and PX-478.

This box summarizes key points contained in the article.

hypoxia-response element (HRE) (5′-RCGTG-3′, where R is A or G) in the promoter region of a number of genes, including glucose transporters, glycolytic enzymes, angiogenic growth factors, and several molecules involved in apoptosis and cell proliferation such as erythropoietin (EPO), transferrin, endothelin-1, iNOS, heme oxygenase 1, VEGF, IGF and IGF-binding proteins [14,15].

Until now, physiological and pathological implications of HIF in various human diseases including inflammation, cardiovascular disorder and cancer have been clarified [16-18]. Especially during cancer development, HIF-1α is a key regulator of the expression of various genes associated with tumor angiogenesis, metastasis, invasion, proliferation and apoptosis. Overexpression of HIF-1α has been observed in human cancers including brain, breast, colon, lung, ovary and prostate cancers [19], and HIF-1α is implicated in treatment resistance and poor prognosis in the hypoxic region around cancer. Therefore, drugs targeting HIF-1α have the potential to target multiple cancer processes, and a large number of HIF inhibitors have been developed. Several HIF inhibitors have entered clinical trials. This survey reviews the patent literature of HIF inhibitors and clinical trials reported in the last 7 years (**Figure 1**).

2. Small molecule HIF inhibitors

2.1 PX-12

Thioredoxin-1 (Trx-1) is a cellular redox protein that promotes tumor growth, inhibits apoptosis and upregulates HIF-1α and VEGF. PX-12 (1-methylpropyl 2-imidazolyl disulfide, compound 1 in **Figure 2**) has shown both excellent *in vitro* and promising *in vivo* antitumor activity, irreversibly thio-alkylating the Cys73 thioredoxin residue [20]. PX-12 inhibition of Trx-1 results in subsequent inhibition of the hypoxia-induced increase in HIF-1α protein and VEGF secretion [21]. PX-12 is rapidly metabolized, providing two inactive metabolites, volatile 2-butanethiol and 2-mercaptoimidazole (**Figure 2**).

PX-12 was tested in Phase I pharmacokinetic and pharmacodynamic study in patients with advanced solid tumors. Thirty-eight patients with advanced solid tumors received PX-12 at doses of 9 – 300 mg/m^2, as 1- or 3 h intravenous infusion on days 1 – 5, repeated every 3 weeks. The best response was stable disease (SD) in seven patients (126 – 332 days). PX-12 treatment lowered plasma Trx-1 concentrations in a dose-dependent manner. PX-12 was tolerated up to a dose of 226 mg/m^2 by a 3 h infusion [22,23]. However, a randomized Phase II study of PX-12 in patients with advanced cancer of the pancreas following progression after a gemcitabine-containing combination resulted in the lack of significant antitumor activity and unexpectedly low baseline Trx-1 levels. PX-12 does not appear to be active in unselected patients with previously treated advanced pancreatic cancer. Thus, the study was terminated [24].

2.2 PX-478

PX-478 (*S*-2-amino-3-[4′-*N*,*N*,-bis(2-chloroethyl)amino]phenyl propionic acid *N*-oxide dihydrochloride, compound 2 in **Figure 2**) suppresses constitutive and hypoxia-induced levels of HIF-1α protein in various cancer cells in a pVHL and p53-independent manner [25].

A patent application from ProlX Pharmaceuticals claimed that *N*-oxides of melphalan derivatives are HIF-1α inhibitors useful for the treatment of diseases associated with HIF, including choroidal and retinal neovascularization, age-related macular degeneration, joint disease, inflammation, neurodegenerative diseases and ischemic neperfusion injury [26]. Various biological data were provided in this patent application. PX-478 inhibited the hypoxia-induced expression of HIF-1α in prostate cancer PC-3, breast cancer MCF-7 and colon cancer HT-29 cells without affecting the HIF-1β level, and IC_{50} values were 2.1, 3.5 and 17.8 μM, respectively. PX-478 also inhibited the hypoxia-induced HIF transactivation in MCF-7 and HT-29 cells with IC_{50} values of 20.5 and 23.1 μM, respectively. Furthermore, IC_{50} values for inhibition of the hypoxia-induced VEGF secretion into the medium was 3.8 and 11.5 μM in MCF-7 and HT-29 cells, respectively. The detailed mechanism of action of HIF-1α inhibition by PX-478 was claimed in another patent application from ProlX Pharmaceuticals [27]. PX-478 inhibited HIF-1α expressions in RCC4 (human renal carcinoma cells lacking the VHL gene), indicating that PX-478 suppresses HIF-1α via a VHL-independent pathway. It has been reported that tumor suppressor p53 binds to HIF-1α allowing recruitment of MDM2, an E3 ubiquitin-ligase, resulting in the degradation of both p53 and HIF-1α [28]. PX-478 suppressed the HIF-1α expression in human colon cancer HCT116$^{-/-}$ cells lacking p53, demonstrating that it is not acting by a p53-dependent mechanism. The inhibition of HIF-1α

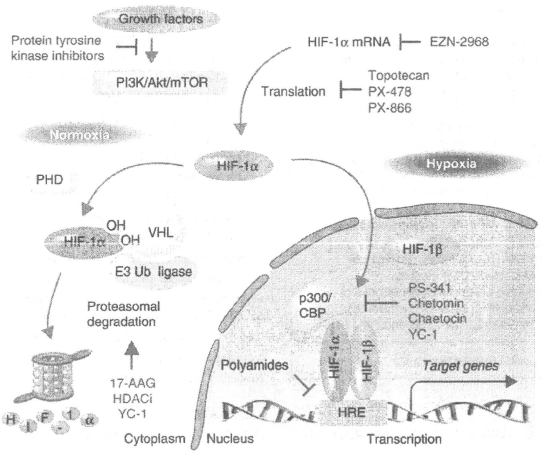

Figure 1. HIF signaling and inhibitors.

expression by PX-478 was proteasome-dependent degradation, and PX-478 increased the level of ubiquitinated HIF-1α through the prevention of deubiquitination of HIF-1α. *In vivo* MCF-7 or HT-29 xenograft model showed that treatment with PX-478 significantly decreased tumor growth and the expression of HIF-1α [26,27,29]. Recently, the Board of Regents of the University of Texas System reported the pharmaceutical compositions of PX-478 for the treatment of small cell lung cancers (SCLC) and the methods of inhibiting metastasis and the combination with radiation, photodynamic therapy and anti-angiogenic agents [30]. PX-478 was effective at both the high (20 mg/kg) and low (10 mg/kg) doses in reducing the tumor volume and weight against the SCLC orthotopic model.

PX-478 was tested in a Phase I, dose escalation study in patients with advanced solid tumors. Forty patients received doses between 1 and 88.2 mg/m^2 orally on days 1 – 5 of a 21 day cycle. Best response was SD in 14/36 evaluable patients. Patients with SD received a median of 4 cycles (range 2 – 16); four patients received ≥ 6 cycles (adenoid cystic, pheochromocytoma, prostate and vaginal cancers). PX-478 has been well tolerated and associated with prolonged SD in patients with advanced cancers. Inhibition of HIF-1α despite low PX-478 levels is consistent with the idea that active metabolites other than melphalan may be responsible for the pharmacodynamic observations. These data support the continued evaluation of HIF-1α inhibition as a therapeutic target [31].

2.3 YC-1 derivatives

YC-1 (3-(5′-hydroxymethyl-2′-furyl)-1-benzylindazole, compound **3** in **Figure 2**) is a soluble guanylyl cyclase (sGC) activator that is primarily developed for the treatment of circulation disorders through inhibition of platelet aggregation and vascular contraction [32,33]. In 2001, Yeo and co-workers found that YC-1 completely blocks the HIF-1α expression at the post-transcriptional level and consequently inhibits the transcription factor activity of HIF under hypoxic condition. In addition, sGC inhibitors did not block the inhibitory effects of YC-1 on HIF, and 8-bromo-cGMP did not inhibit the hypoxia-induced expression of HIF [34]. These results indicate that the inhibition of HIF by YC-1 is sGC-independent action. Thus, YC-1 is recognized as an HIF inhibitor and antitumor agent.

A patent application from HIF Bio, Inc. claimed the use of YC-1 and its derivatives for the inhibition of HIF-1α expression in tumors, including hepatoma, stomach carcinoma, renal carcinoma, cervical carcinoma and neuroblastoma [35]. YC-1 inhibited the hypoxia-induced expression of HIF-1α and its target genes include VEGF, aldolase A and enolase 1 in various cancer cells such as Hep3 G hepatoma, NCI-H87 gastric carcinoma, SiHa cervical, SK-N-MC neuroblastoma and Caki-1 renal carcinoma cells. Almost complete inhibition was observed at the concentration of 10 μM. In the *in vivo* tumor xenograft model, treatment with 30 mg/kg of YC-1 suppressed the growth of tumor cells. In this model, immunohistochemical analysis with tumor

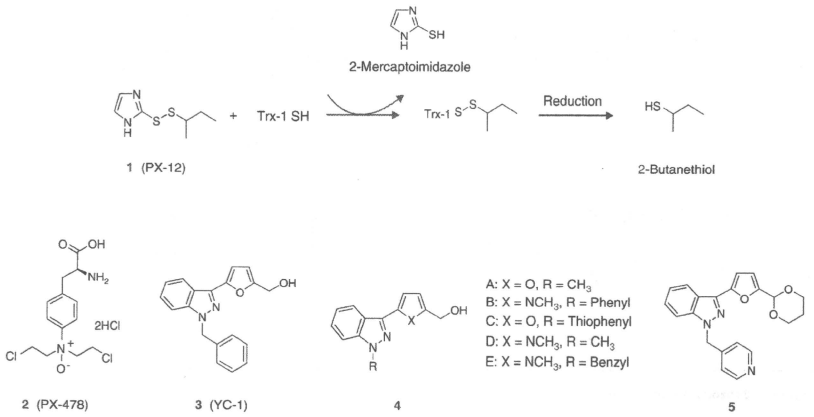

Figure 2. PX-12, PX-478 and YC-1 derivatives.

sections showed that YC-1 reduced the amount of HIF-1α-positive cells and endothelial marker CD31-positive cells. These results indicate that the tumor growth inhibition by YC-1 is mediated by suppression of HIF-1α expression. This application also claimed the use of YC-1 and its derivatives in combination with other anticancer agents. HIF Bio further claimed a series of YC-1 derivatives (compounds **4A–D** in **Figure 2**) [36]. Under hypoxic condition, compounds **4A–D** suppressed the hypoxia-induced expression of HIF-1α similar to YC-1 at the concentration range of 0.3 – 10 μM. The ability of the compounds to inhibit tumor growth was determined in male nude mice following subcutaneous injection of Hep3B hepatoma cells. After the xenografted tumors reached 100 – 150 mm^3 in size, compounds were treated by intraperitoneal injection daily for 2 weeks. At the end of the treatment period, compounds reduced the tumor size from about 900 mm^3 in vehicle-treated controls to about 400 mm^3 at doses of 10 mg/kg/day (compounds **4A-D**) or 30 mg/kg/day (compounds **4A** and **B**). Another patent application from HIF Bio claimed to have a series of heterocycle-substituted pyrazoles, such as compound **5** (**Figure 2**), for the treatment of HIF-related and VEGF-mediated disease or disorder [37]. However, no biological data were presented.

2.4 Benzopyran derivatives

A series of 2,2-dimethyl-2*H*-chromene (2,2,-dimethylbenzopyran) derivatives has been developed as inhibitors of the HIF-1 pathway. The first examples of benzopyran-based HIF-1 inhibitors were patented by researchers from Emory University and Scripps Research Institute in 2004 [38]. These novel benzopyrans were tested for their inhibitory activity on the HIF-1–HRE pathway using LN229 glioma cells expressing the alkaline phosphatase reporter gene. The most potent compound **6** (**Figure 3**) displayed an IC_{50} value of 7.5 μM. Following this first patent, the same group reported an additional series of 2,2-dimethylbenzopyran derivatives in 2007 [39]. A library of 2,2-dimethylbenzopyran derivatives (> 10,000) were prepared by combinatorial synthesis [40-42]. Screening of the library in the cell-based HIF-1–HRE assay resulted in the discovery of highly potent HIF-1 inhibitors, such as KCN-1 (compound **7** in **Figure 3**) with an IC_{50} value of ~ 4 μM. Further analysis showed that KCN-1 reduced hypoxic levels of HIF-1α in glioma cell lines without significantly affecting the levels of HIF-1β. For *in vivo* pharmacological evaluation, KCN-1 was evaluated in nude mice with sc LN229 glioma xenograft implants. A strong and sustained inhibition of tumor growth was observed without any significant weight changes or behavioral abnormalities after intraperitoneal administration of KCN-1 at a dose of 60 mg/kg for 5 days. Further structural optimization provided detailed SAR information. In short: i) dimethoxy substitution on the left-hand phenyl is preferred, ii) amide or aliphatic bond is also permitted in place of sulfonamide, iii) flexible rings are favored over *N*-aromatic rings and flexible aliphatic chains are preferred and iv) addition of hydrophilic groups is tolerated on benzopyran. More recently, structurally related 2,2-benzopyran derivatives (compounds **8** and **9** in **Figure 3**) were also shown to inhibit the HIF-1–HRE pathway [43,44].

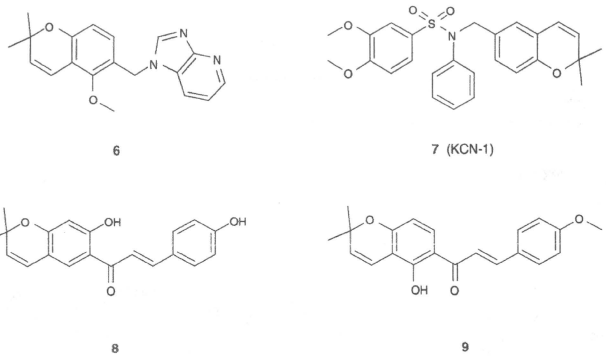

Figure 3. Benzopyran derivatives.

2.5 Aromatic compounds and heteroaryls

Due to the complexity of the biological processes that regulate the HIF-1 pathway, a wide variety of structural motifs have been reported to inhibit HIF-1 activity. For example, a group from the National Cancer Institute evaluated numerous tricyclic compounds using HIF-1 reporter luciferase assay in recombinant U251 human glioma cells [45]. One of the examples (NSC 644221, compound **10** in **Figure 4**) originally reported as a weak DNA-binding intercalating agent [46] was further evaluated and shown to decrease hypoxic induction of luciferase expression in a dose-dependent fashion (EC_{50} ~ 1 μM) in the U251-HRE cell assay [47]. The specificity on HRE was clearly indicated by the fact that NSC 644221 did not significantly affect the constitutive luciferase expression in the control cell line U251-pGL3 up to 10 μM. Interestingly, it was shown that NSC 644221 did not inhibit the HIF-1α expression when cells were transfected with siRNA targeting topoIIa.

Novel thiazolidinone compounds were claimed by Cell Therapeutics Europe S.R.L. to inhibit HIF-1α–p300 interaction and prevent VEGF production in tumor cells under hypoxia conditions. One of the examples (compound **11** in **Figure 4**) demonstrated its ability to disrupt HIF-1α–p300 interaction with an IC_{50} value of 1.4 μM in a fluorescence assay (DELIFIA™) [48].

The University of Texas reported that imidazo[1,2-a] pyrazine-based tyrosine kinase inhibitors, exemplified by compound **12** (**Figure 4**), inhibited HIF-1 expression and HIF-signal transduction pathways [49]. Influence of these tyrosine kinase inhibitors on HIF was tested on C6#4 cells. Compound **12** showed EC_{50} values of 2.2 and 19.6 μM with respect to G/R (GFP/RFP expression, HIF-1α inhibitory activity) and WST-1 (cell viability).

In a patent application filed by Piramal [50], small molecule compounds that contain the 2-chloro-*N*-pyridin-3-ylacetamide moiety were tested in U251 human glioma cells stably transfected with human HRE and the U251 pGL3 cells (control cell line). Specificity index (SI) and the ratio of IC_{50} under normoxic condition to hypoxia condition were measured for selected compounds in the patent. One of the examples (compound **13A** in **Figure 4**) exhibited SI > 20 in the assay. Recently, a related analog was reported as P2630 (compound **13B**) [51]. P2630 exhibited strong HIF-1α inhibitory activity under hypoxic (1% O_2) conditions with an IC_{50} value of 0.8 μM and marginal inhibitory activity under normoxic (21% O_2) conditions. Anti-proliferative activity was tested in ^{3}H-thymidine incorporation assay across different cancer cell lines (PC-3, DU-145, U251, HCT-116, Ovcar-3 and Panc-1) and normal cell lines (MRC-5 and WI-38). P2630 showed best anti-proliferative activity in the PC-3 cell line (IC_{50}: 1.0 μM), while it did not potently inhibit the proliferation of normal cell lines (IC_{50}: > 10 μM for MRC-5; 6.5 μM for WI-38). *In vivo* efficacy was evaluated in the SCID mice with PC-3 xenograft. After a 19-day oral administration (50 mg/kg twice daily), P2630 demonstrated significant tumor growth inhibition without substantial weight loss.

Thalidomide analogs were previously reported to possess anti-angiogenic activity in a HUVEC assay [52]. In 2008, Charlesson LLC claimed that the thalidomide analogs were suppressors of HIF-1α expression and useful for the treatment of vascular abnormalities such as neovascularization and vascular leakage [53]. The thalidomide analogs in this patent significantly suppressed the HIF-1α expression in PC-3 prostate cancer cells by ~ 79 – 90% at the tested concentration (10 μM). According to the data demonstrated in this patent, the thalidomide analogs have promising effects for the

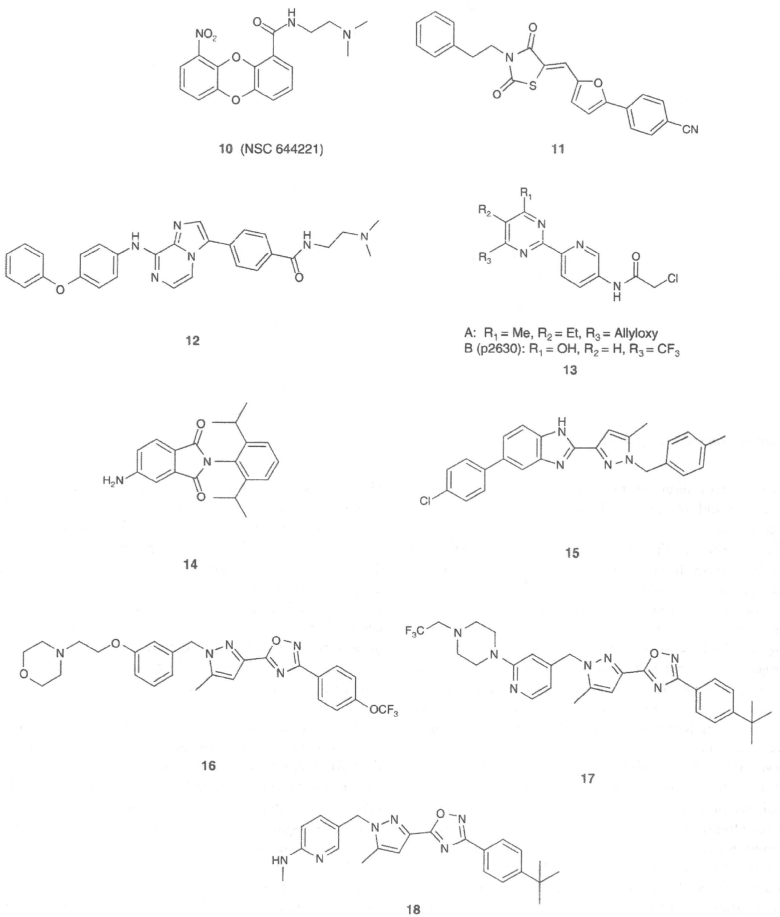

Figure 4. Aromatic compounds and heteroaryls.

treatment of ocular disease, particularly diabetic retinopathy. CLT-003 (compound 14 in **Figure** 4) was intravitreally injected (5 µl/eye, 0.8 mM in BN rat serum) to the right eye and the same volume of vehicle was injected to the left eye of streptozotocin-treated diabetic rats. Measurement of retinal vascular permeability by Evans blue-albumin method after 2 days of injection showed that CLT-003 significantly reduced retinal vascular leakage by 100% (n = 6). CLT-003 has been developed as a clinical candidate by Charlesson LLC to primarily target diabetic macular edema.

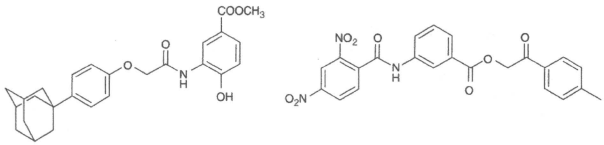

19 20 (FMG19G11)

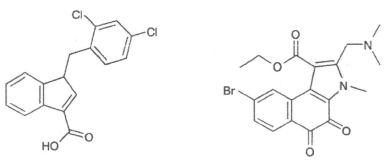

21 22

Figure 4. Aromatic compounds and heteroaryls (continued).

For secondary indications, macular edema secondary to other pathologies and wet age-related macular degeneration are also suggested [54].

Bayer Schering Pharma disclosed a patent application describing novel heteroaryl-substituted pyrazole compounds as modulators of HIF-1α for the treatment of hyperproliferative disorders and diseases associated with angiogenesis [55]. These pyrazole derivatives were tested in HIF-luciferase assay using HCT-116 cells. One of the examples (compound **15** in **Figure 4**) exhibited an IC_{50} value of 0.003 μM in the assay. Recently, they disclosed an additional series of novel pyrazole derivatives, especially 5-(5-methyl-1*H*-pyrazol-3-yl)-1,2,4-oxadiazole analogs (compounds **16 – 18** in **Figure 4**) as highly potent HIF inhibitors [56-58]. Some of these pyrazole derivatives showed very strong inhibition toward HIF-1 transcriptional activity in the luciferase assay with IC_{50} values in the range of sub-nanomolar.

Korea Research Institute of Bioscience and Biotechnology claimed novel aryl and heterocyclic derivatives as HIF inhibitors for the treatment and prevention of cancer [59]. Compound **19** (**Figure 4**) inhibited the hypoxia-induced accumulation of HIF-1α and the expression of HIF-1 target genes EPO and VEGF without affecting HIF-1β expression in human hepatocellular carcinoma cell lines Hep3B. Administration of compound **19** at the dose of 20 or 50 kg/ml inhibited the growth of tumor in the MDA-MB-435 implanted nude mouse model. Recently, the action mechanism of compound **19** has been reported to promote proteasomal degradation of HIF-1α through upregulation of VHL [60]. Furthermore, Lee *et al.* reported inhibitory effects of (aryloxyacetylamino)benzoic acid analogs on HIF-1 transcriptional activity [61] and found that the benzimidazole analog is a novel HIF inhibitor that regulates the stability of HIF-1α through the heat-shock protein (HSP) 90-Akt pathway, leading to the degradation of HIF-1α [62]. The ortho-carborane analogs of compound **19** were reported as potent inhibitors of the hypoxia-induced activation of HIF [63]. The detailed mechanistic study using their chemical probes revealed that the target molecule of the ortho-carborane analogs was identified to be HSP60 [64].

A group from Centro de Investigacion Principe Felipe claimed that a series of benzamide derivatives could modulate and/or inhibit the transcription of genes modulated by HIF [65]. Screening of approximately 12,000 compounds using luciferase reporter gene-based assay containing 9 repetitions of the HRE 5′ upstream of the start codon in the active promoter region constitutively expressed in the HeLa cell line (HeLa-9x-HRE-Luc) resulted in the discovery of FMG19G11 (compound **20** in **Figure 4**) [66]. This compound was shown to reduce hypoxia-induced luciferase activity with an IC_{50} value of 80 nM in the HeLa-9x-HRE-Luc assay. While specific data were not shown, it was suggested that FMG19G11 inhibited transcriptional activity of HIFα not only in HeLa cell line but also in adult human cell lines from various tissues such as colon HT-29 and the breast cancer cell line MDA-MB-435-S. Notably, FM19G11 had a similar effect on HIF regulation in stem cells. Further experiments revealed that FMG19G11 demonstrated dose-dependent inhibitory activity on HIFα protein accumulation in adult rat epSPC. As for toxicity, FMG19G11 did not show any cytotoxicity on the HeLa cell line up to 30 μM in the standard oxygen tension or 50 μM under hypoxic conditions. Recent publication from

the same group reported that FMG19G11, in response to rapid hyper-activation of the growth signaling pathway through mTOR, triggered a DNA damage response associated with G(1)/S-phase arrest in a p53-dependent fashion [67].

A series of lonidamine analogs were claimed by Threshold Pharmaceuticals to be HIF-1α inhibitors [68]. The anticancer drug lonidamine (compound 21 in **Figure 4**) inhibited the hypoxia-induced HIF-1α expression in nuclear and whole cell extract of LNCaP and PC-3 cells at the concentration range of 100 – 600 μM, and a complete inhibition was observed at 400 μM.

A patent application from Cell Therapeutics Europe S.R.L. claimed that novel indole derivatives inhibit the interaction between HIF and its co-activator p300 [69]. Among the indole derivatives, compound 22 (**Figure 4**) prevented binding of HIF and p300 with an IC_{50} value of 1.5 μM, and showed the most potent inhibitory activity in VEGF-luciferase Hep3B cells with an IC_{50} value of 0.26 μM.

3. Steroidal HIF inhibitors

A patent application from Bionaut International claimed a series of steroidal compounds as HIF inhibitors [70]. Results from the screening of anti-neoplastic agents with thousands of compounds showed that cardiac glycosides, redox effectors and steroid signal modulators were highly effective agents for the treatment of neoplastic disorder, particularly HIF-positive tumor cells, pancreatic, lung, colon, prostate, cervical, renal, uterine and breast cancers. Among the cardiac glycosides including ouabain, digitoxigenin, digoxin and lanatoside C, ouabain (compound 23 in **Figure 5**), also known as strodival, potently inhibited HIF-responsive reporter activity in NSCLC A549 cell lines. Also, additive effects were observed by a combination of ouabain with redox effector niclosamide [70]. As ouabain had been identified as a Na^+/K^+ ATPase inhibitor, another patent claimed that Na^+/K^+ ATPase inhibitors such as proscillaridin (compound 24 in **Figure 5**), also known as talusfn, and marinobufagenin can be used either alone or in combination with other anticancer agents for more effective treatment of refractory cancer including pancreatic cancer [71-74]. Both proscillaridin and ouabain strongly inhibited the hypoxia-induced increase in the level of HIF-1α and production of VEGF in A549 cells. The action mechanism of HIF-1α inhibition by the cardiac glycoside compounds was described as the production of reactive oxygen species (ROS) which leads to the ubiquitylation and degradation of HIF-1α. Ouabain induced ROS in various cancer cells including A549, Caki-1 and Panc-1 cells. Also, catalase inhibited the ouabain-mediated reduction of HIF-1α protein, indicating that ouabain inhibits the HIF-1α expression through an increase in ROS production. Panc-1 implanted xenograft in a nude mouse model showed that administration of ouabain almost completely inhibited tumor growth and that additive antitumor activity was observed by co-administration with anticancer agent gemcitabine [73,74]. In 2007, Bionaut International further reported several steroidal HIF modulators including bufalin, digitoxigenin, digoxin, lanatoside C, strophantin K, uzarigenin, ouabain and proscillaridin, and their use for treatment of ocular disorders including angiogenic ocular disease, ocular inflammation, diabetic retinopathy, corneal graft rejection, glaucoma, ocular edema, cataracts, conjunctivitis and sickle cell retinopathy [75]. In human retinal pigment epithelial ARPE-19 cells, proscillaridin was more potent than ouabain in inhibiting the hypoxia- or IGF-1-induced expression of HIF-1α protein. Furthermore, proscillaridin inhibited the hypoxia-induced expressions of angiogenic factors include VEGF, TIMP and angionenin with IC_{50} values of 32.5, 12.9 and 4.5 nM, respectively, and showed the ability to prevent choroidal neovascularization at a concentration of 60 ng/ml in serum [75]. Also, another steroidal HIF inhibitor, compound 25 (**Figure 5**), was patented by Bionaut International [76]. Similar to the other steroidal HIF inhibitors previously claimed, compound 25 inhibited the hypoxia-induced expression of HIF-1α in Panc-1, Caki-1 and A549 cells, and gave 83% inhibition of tumor growth at 15 mg/ml in a Caki-1 cells implanted xenograft nude mouse model [77]. SRI International also claimed a series of bufadienolide derivatives (R is the nitrogen-containing C_{2-6} heterocyclyl group, such as compound 26 in **Figure 5**) as an HIF modulator for treatment of HIF-1-mediated diseases, particularly neoplastic disorders. However, no detailed biological results were provided.

Another patent application from SRI International claimed a series of substituted l, 3, 5 (10)-estratrienes as steroidal anti-angiogenic and anti-HIF compounds for the treatment of cancer, corneal graft neovascularization, diabetic retinopathy, psoriasis and rheumatoid arthritis [78]. SR-16388 (citrate salt form of compound 27 in **Figure 5**) potently inhibited the hypoxia-induced expression of HIF-1α protein in human prostate cancer PC-3 cells and human breast cancer MDA-MB-231 cells, but did not affect normal cell lines, RAW264.7 macrophages. Additionally, the specific data of anti-angiogenic activity were provided for SR-16388. Among the claimed substituted l, 3, 5 (10)-estratrienes, SR-16388 most potently inhibited the proliferation of human dermal microvascular endothelial cells and the IC_{50} value was about 80 nM. Wound healing experiment showed that a dose of 3 – 30 mg/kg SR-16388 potently inhibited the formation of granulation tissue and resulted in a 30% decrease in microvessel formation as compared to the control group. Furthermore, SR-16388 was active in the inhibition of the proliferation of various types of cancer cells including lung, brain, ovarian, prostate and breast cancers in the range of 0.1 – 1 μM. The results from the PC-3 cells implanted xenograft nude mouse model showed that the oral treatment of 10, 30 and 100 mg/kg SR-16388 markedly reduced tumor growth rates compared to the untreated control group and that microvascularization in the group treated with 30 mg/kg